RSC Advances

PAPER

View Article Online
View Journal | View Issue



Cite this: *RSC Adv.*, 2020, **10**, 36794

# Hydrothermal-template synthesis and electrochemical properties of $Co_3O_4$/nitrogen-doped hemisphere-porous graphene composites with 3D heterogeneous structure†

Haiyang Fan,[ab] Guiyun Yi,*[ab] Qiming Tian,[ab] Xiuxiu Zhang,[ab] Baolin Xing,*[bc] Chuanxiang Zhang,[ab] Lunjian Chen[ab] and Yulong Zhang[ab]

Received 10th August 2020
Accepted 29th September 2020

DOI: 10.1039/d0ra06897g

rsc.li/rsc-advances

Despite the high capacity of $Co_3O_4$ employed in lithium-ion battery anodes, the reduced conductivity and grievous volume change of $Co_3O_4$ during long cycling of insertion/extraction of lithium-ions remain a challenge. Herein, an optimized nanocomposite, $Co_3O_4$/nitrogen-doped hemisphere-porous graphene composite ($Co_3O_4$/N-HPGC), is synthesized by a facile hydrothermal-template approach with polystyrene (PS) microspheres as a template. The characterization results demonstrate that $Co_3O_4$ nanoparticles are densely anchored onto graphene layers, nitrogen elements are successfully introduced by carbamide and the nanocomposites maintain the hemispherical porous structure. As an anode material for lithium-ion batteries, the composite material not only maintains a relatively high lithium storage capacity (the first discharge specific capacity can reach 2696 mA h $g^{-1}$), but also shows significantly improved rate performance (1188 mA h $g^{-1}$ at 0.1 A $g^{-1}$, 344 mA h $g^{-1}$ at 5 A $g^{-1}$) and enhanced cycling stability (683 mA h $g^{-1}$ after 500 cycles at 1 A $g^{-1}$). The enhanced electrochemical properties of $Co_3O_4$/N-HPGC nanocomposites can be ascribed to the synergistic effects of $Co_3O_4$ nanoparticles, novel hierarchical structure with hemisphere-pores and nitrogen-containing functional groups of the nanomaterials. Therefore, the developed strategy can be extended as a universal and scalable approach for integrating various metal oxides into graphene-based materials for energy storage and conversion applications.



## 1. Introduction

To address the problems of depleting fossil fuels and global warming, there is an urgent need to develop energy storage devices with high-power density that can store and supply electricity.[1] Lithium-ion batteries (LIBs), as a new generation of environmental-friendly electrochemical energy storage and conversion device, have been widely used in portable electronic devices, static energy storage systems and electric bicycles due to their advantages of high energy density, long cycle life and high discharge voltage.[2–4] However, traditional LIBs using graphite electrodes with a low theoretical specific capacity (372 mA h $g^{-1}$) cannot meet the ever-growing demands for high performance.[5] Recently, organic materials (azobenzene-4,4′-dicarboxylic acid lithium salt, and dithianon) with the advantages of light weight, abundance, low cost, sustainability, and recyclability have become desirable for green and sustainable LIBs but the poor cycle stability and low power density limit their large-scale application.[6,7] Therefore, persistent efforts have been devoted to exploiting new anode materials, which can enhance their rate capability, energy density and cycling stability.

As anode materials of next generation LIBs, transition metal oxides (TMOs) have attracted significant attention due to their higher theorical capacity than traditional graphite.[8,9] Among these TMOs, $Co_3O_4$ has been recognized as a potential candidate of anode material for LIBs owing to its high theoretical specific capacity of 890 mA h $g^{-1}$ than that of $TiNb_2O_7$ (387.6 mA h $g^{-1}$), CuO (674 mA h $g^{-1}$) and $SnO_2$ (780 mA h $g^{-1}$),[10] which is based on the following reaction equation:[11–13]

$$Co_3O_4 + 8Li^+ + 8e^- \rightleftharpoons 3Co + 4Li_2O \quad (1)$$

However, the practical application of $Co_3O_4$ has been limited because of its low inherent electrical conductivity, poor rate capability and severe particle agglomeration during the

[a]Henan Key Laboratory of Coal Green Conversion, College of Chemistry and Chemical Engineering, Henan Polytechnic University, Jiaozuo 454003, China. E-mail: ygyun@hpu.edu.cn

[b]Collaborative Innovation Center of Coal Work Safety of Henan Province, Jiaozuo 454003, China. E-mail: baolinxing@hpu.edu.cn

[c]Henan Province Industrial Technology Research Institute of Resources and Materials, Zhengzhou University, Zhengzhou 454001, China

† Electronic supplementary information (ESI) available. See DOI: 10.1039/d0ra06897g

repeated charge/discharge cycling, which can result in the pulverization of electrodes, poorer cycling stability and more capacity loss.[14,15] Hence, several efforts have been devoted to circumvent these troublesome drawbacks. For example, the hybrid nanomaterials consisting of nanostructured $Co_3O_4$ and carbonaceous matrix (graphene,[16,17] carbon nanotubes[18,19] and carbon nanowires[20]) were synthesized. It is noteworthy that graphene-based nanomaterials can be a promising candidate for the recombination with $Co_3O_4$ because they can serve as buffer against volume expansion and enhance the electrical conductivity of the anode electrodes.[21] Additionally, the graphene-based materials possess high thermal conductivity and chemical stability, which offer significant accessional advantages.[22] Nulu Venugopal[23] *et al.* exhibited that $Co_3O_4$ hybridized with carbon nanotubes can act as an anode material of LIBs with a lithium ion storage capacity of 602 mA h $g^{-1}$ at 500 mA $g^{-1}$. Dou[24] *et al.* revealed that $Co_3O_4$/graphene composite displayed a superior endurance during thousands of charge/discharge cycles when it was used as an active material of LIBs. Sun[25] *et al.* indicated that mesoporous $Co_3O_4$ nanosheets-3D graphene networks (3DGN) hybrid materials have been synthesized and investigated as anode materials for Li-ion batteries (LIBs). Consequently, coupling $Co_3O_4$ with other functional materials has been confirmed to be an effective strategy to improve the electrochemical properties.

Besides, doping is another efficient approach for enhancing electrochemical performance. Recently, nitrogen-doped graphene-based composite has been investigated as a significant research hotspot, because the incorporation of nitrogen elements into graphene can effectively enhance the electrochemical performance of carbon-based materials. The doping of nitrogen can not only induce numerous defects, but also form a disordered structure of carbon-based materials, which can provide more active sites to improve the lithium ions storage capacity.[26] Additionally, the presence of nitrogen heteroatoms also can promote the electrical conductivity, interfacial stability and reactivity of the carbon-based nanomaterials, which is beneficial to enhancing the rate capability and facilitating its reaction kinetics of working electrodes in storing energy.[27] Moreover, for the carbon-based anode nanomaterials, the porous structure can shorten the transport length of lithium-ions and promote the reaction of charge-transfer on the electrode/electrolyte interface, which is capable of offering excess high lithiation capability.[28] Hence, it is expected that compounding $Co_3O_4$ with N-doped carbon materials should be a promising strategy to increase the electrical conductivity, promoting the reaction kinetics and maintain the structure, thus reaching a significant storage of lithium ions.

Herein, anode electrodes ($Co_3O_4$/N-HPGC) consisting of $Co_3O_4$ and nitrogen-doped hemispherical porous graphene were synthesized by a hydrothermal-template approach with polystyrene (PS) microspheres as the template. Several characterization techniques have been employed to explore the structure, morphology and physicochemical properties of the $Co_3O_4$/N-HPGC composites. Benefiting from the desirable unique structure and advanced nitrogen doping, the as-synthesized $Co_3O_4$/N-HPGC nanocomposite, examined as electrode materials for LIBs, exhibits high lithium storage capacity, good rate performance and excellent cycling stability, which can be one of the most promising candidates for LIBs anode materials.

## 2. Results and discussion

### 2.1. Structural characterization

The structure and morphology of HPGC and $Co_3O_4$/N-HPGC nanocomposite were investigated by TEM (Fig. 1). As can be

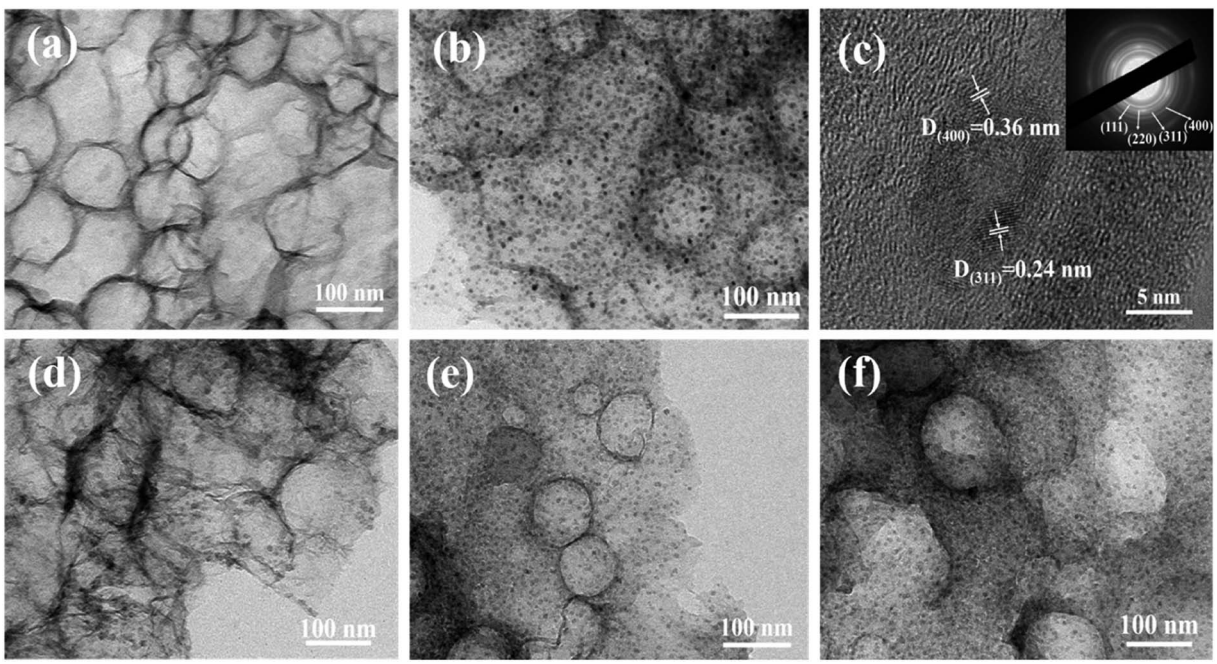


Fig. 1 TEM images of (a) HPGC and (b and d–f) $Co_3O_4$/N-HPGC-2, 1, 3 and 4, (c) HRTEM and SAED images of $Co_3O_4$/N-HPGC-2.

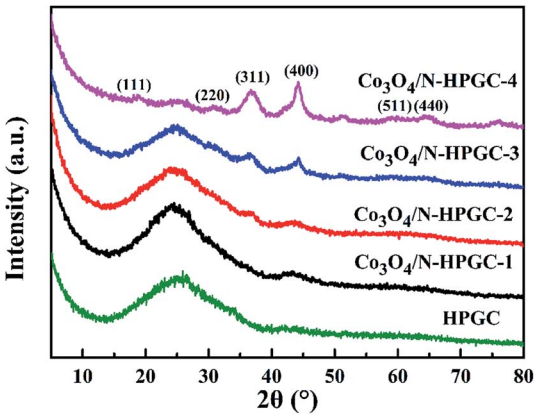


Fig. 2 XRD patterns of HPGC, $Co_3O_4$/N-HPGC-1, 2, 3 and 4.

seen, the TEM image of composite without $Co_3O_4$ loads (Fig. 1a) reveals a hemispherical superimposed structure, formed due to the removed PS microsphere template, resulting in the self-assembly process of RGO. According to Fig. 1b and d–f, the nanocomposites loaded with $Co_3O_4$ particles still maintain the hemispherical pore structure after removing the PS microsphere template, which undoubtedly increases the specific surface area of the complex. Additionally, the $Co_3O_4$ nanoparticles are tightly anchored onto the surface of RGO sheets. However, the increase of $Co_3O_4$ loadings renders the nanoparticles more densely dispersed and simultaneously results in partial agglomeration. The HRTEM image (Fig. 1c) of $Co_3O_4$/N-HPGC-2 nanocomposite indicates that the presence of 0.36 nm and 0.24 nm interlayers spacing coincides with the (400) and (311) lattices spacing of $Co_3O_4$, meanwhile, the size of particles is measured to be between 5 and 12 nm. Furthermore, the SAED patterns (Fig. 1c) indicates that the diffraction rings sequentially corresponds to the (111), (220), (311) and (400) crystal planes of $Co_3O_4$, which provides further evidence that $Co_3O_4$ nanoparticles are successfully loaded onto RGO layers without noticeable impurity formation.[29]

The XRD patterns of composites with different $Co_3O_4$ loads are illustrated in Fig. 2. For HPGC and $Co_3O_4$/N-HPGC-1, 2, 3 composites, the broad peak appears at about 26.5°, corresponding to (002) diffraction mode of graphene structure, which is the characteristic of nitrogen-doped hemisphere-porous graphene. It can be found that the diffraction peaks of the $Co_3O_4$/N-HPGC nanocomposites at $2\theta = 19°$, 31.2°, 36.7°, 44.2°, 59.4° and 65.6° are recognized to the diffraction of (111), (220), (311), (400), (511) and (440) planes of the spinel $Co_3O_4$ with face-centered cubic phase (JCPDS no. 42-1467),[13] respectively. Additionally, compared with HPGC, the characteristic peaks coincided with $Co_3O_4$ in the sample become more obvious; meanwhile, the (002) diffraction peak of graphene decreases gradually with the amount of cobalt nitrate increasing. Therefore, the XRD analysis confirms the $Co_3O_4$ nanoparticles were uniformly immobilized on the hemisphere-porous graphene sheets, which corresponds to the TEM analysis.

Raman spectroscopy was performed to study the nature of graphitization of as-prepared samples. As shown in Fig. 3a, the peaks appeared at 1349 $cm^{-1}$ and 1592 $cm^{-1}$ are corresponded to the D band (disordered carbon) and G band (graphitized carbon), which is attributed to the disordered structure or edge defects and $sp^2$-hybridized carbon atoms of crystalline graphite, respectively.[30] Moreover, the peak at 621 $cm^{-1}$ in $Co_3O_4$/N-HPGC-2 nanohybrids is observed, which can be assigned to the characteristic peak of crystalline of $Co_3O_4$.[31] Generally, the intensity ratio ($I_D/I_G$) of D and G bands can provide the structural change information of nanocarbon materials, and a high $I_D/I_G$ ratio indicates a high extent of disordered structure.[32] The $I_D/I_G$ of $Co_3O_4$/N-HPGC-2 is 1.066, higher than 0.996 of HPGC, indicating a higher density of defect sites due to the porous structure and nitrogen doping, which confirms the coexistence of $Co_3O_4$ amorphous carbon and N-doping.[33] The TGA curve of $Co_3O_4$/N-HPGC-2 was shown in Fig. 3b. The first low-temperature weight loss under 200 °C is primarily due to the desorption of physically and adsorbed water.[34] The second weight loss step in the range of 200–600 °C is mostly ascribed to

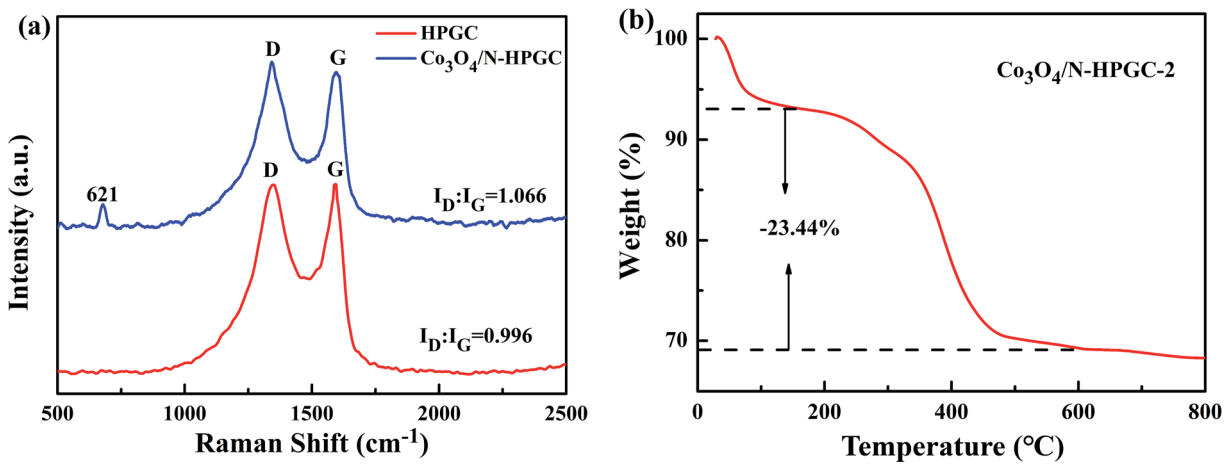


Fig. 3 (a) Raman spectra of HPGC and $Co_3O_4$/N-HPGC-2 (b) TGA curve of $Co_3O_4$/N-HPGC-2.

 

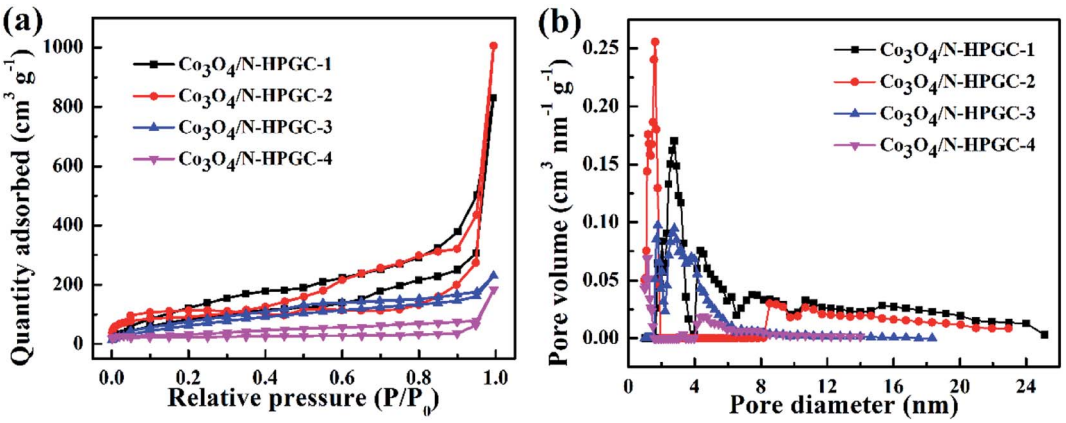


Fig. 4 (a) $N_2$ adsorption and desorption curve and (b) pore size distribution curve of $Co_3O_4$/N-HPGC-1, 2, 3, 4.

the burning of N-doped graphene and the remnants after 600 °C should be attributed to $Co_3O_4$. Based on the TGA curve, the weight percentage of HPGC in $Co_3O_4$/N-HPGC-2 is around 23.44 wt%.

The specific surface area and pore size distribution of $Co_3O_4$/N-HPGC nanocomposite were calculated by $N_2$ adsorption–desorption measurements and BET analysis. The $N_2$ adsorption–desorption isotherm is shown in Fig. 4 and the pore structure parameters are listed in Table 1. According to Fig. 3a, it is observed that the isotherms of all composites can be classified as type IV isotherms with H3 hysteresis loop, which is mainly attributed to wedge-shaped holes formed by layers of graphene and the presence of hierarchical pores.[35] Additionally, as shown in Fig. 4b, the pore size distribution based on BJH method reveals that the existence of some micropores, mesopores and a few hemisphere macropores formed by the removed polystyrene (PS) microspheres templates, and the aperture distribution range gradually narrows due to the overmuch $Co_3O_4$ loadings. The excessive loads will easily induce the agglomeration of $Co_3O_4$ particles and clog the pores of samples, which can reduce the specific surface area of the composites.[36] Moreover, the BET specific surface area of $Co_3O_4$/N-HPGC-1, 2, 3, 4 are listed in Table 1. With the increase of the $Co_3O_4$ loading capacities, the specific surface area of $Co_3O_4$/N-HPGC-2 nanomaterials can reach the maximum of 348 $m^2\ g^{-1}$. While when the loadings further increase, the surface area gradually decreases to the minimum of 117 $m^2\ g^{-1}$. The higher surface area of $Co_3O_4$/N-HPGC-2 nanohybrids may be ascribed to the distribution of these hierarchical pores. Thus, it is conductive to electrolyte diffusion to the active sites, and can effectively enhance the storage of lithium-ions during charge/discharge, contributing to the application of $Co_3O_4$/N-HPGC composite materials in LIBs.

According to $N_2$ adsorption–desorption results, the $Co_3O_4$/N-HPGC-2 possesses the highest specific surface area, thus the electronic structure and chemical composition of $Co_3O_4$/N-HPGC-2 composites are further analyzed by XPS, and the results are shown in Fig. 5. From the full spectrum (Fig. 5a) of $Co_3O_4$/N-HPGC-2 nanocomposite, it can be observed that in addition to the three peaks of O 1s, N 1s and C 1s, there is also the characteristic peak of Co 2p at 780.5 eV, indicating that Co has been successfully doped into graphene. According to the analysis of the Co 2p high-resolution energy level spectrum (Fig. 5b), the two main peaks at 795.9 eV and 780.5 eV can be attributed to Co $2p_{1/2}$ and Co $2p_{3/2}$ spin orbital peaks of $Co_3O_4$, respectively, which illustrates Co element exists in the form of $Co_3O_4$ and is compounded with HPGC material.[37,38] The spin-energy separation is 15 eV with the characteristic of a $Co_3O_4$ phase, which indicates the presence of $Co^{2+}$ and $Co^{3+}$ species in the composites and is in accordance with the previous reports.[39] As shown in Fig. 4c, the main peak centered at 284.7 eV is related to the C–C group of graphite carbon. The peak at 285.2 eV reflects the bonding structure of the C–N bonds, corresponding to the N–$sp^2$ C bonds, which may originate from substitution of N atoms and defects or the edge of the nitrogen doped graphene.[40] And the weak peak appeared at 286.1 eV is ascribed to C–O group of the nanocomposites. Additionally, the high-resolution N 1s spectra (Fig. 5d) displayed four peaks located at 398.7 eV, 400.2 eV, 401.1 eV and 406.2 eV, which are attributed to pyridinic-N (a N atom bonding with two C atoms),

Table 1 Pore structure parameters of $Co_3O_4$/N-HPGC composites

| Sample | $S_{BET}$ ($m^2\ g^{-1}$) | $V_t$ ($cm^3\ g^{-1}$) | $V_{mic}$ ($cm^3\ g^{-1}$) | $V_{mes}/V_t$ (%) |
|---|---|---|---|---|
| $Co_3O_4$/N-HPGC-1 | 337 | 1.284 | 0.004 | 99.69 |
| $Co_3O_4$/N-HPGC-2 | 348 | 1.555 | 0.314 | 79.81 |
| $Co_3O_4$/N-HPGC-3 | 226 | 0.357 | 0.079 | 78.87 |
| $Co_3O_4$/N-HPGC-4 | 117 | 0.285 | 0.101 | 64.60 |

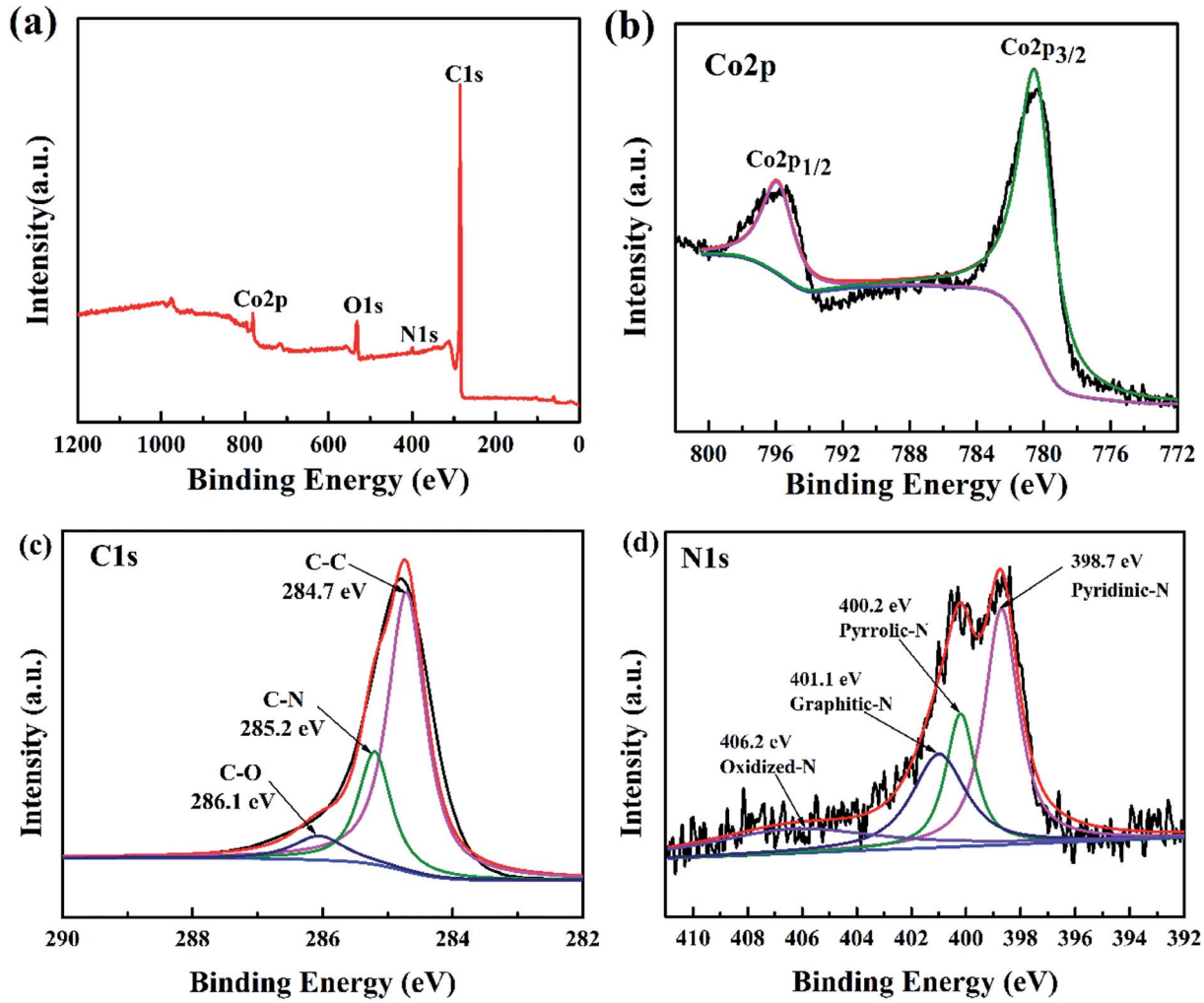


Fig. 5 (a) XPS survey spectra of $Co_3O_4$/N-HPGC-2 and high-resolution XPS spectra of (b) Co 2p, (c) C 1s, (d) N 1s of $Co_3O_4$/N-HPGC-2.

Table 2 Relative atomic percentages in $Co_3O_4$/N-HPGF-3 analyzed based on the XPS spectra

| Sample | C 1s (%) | O 1s (%) | N 1s (%) | Co 2p (%) |
|---|---|---|---|---|
| $Co_3O_4$/N-HPGC-2 | 89.89 | 7.24 | 1.74 | 1.13 |

pyrrolic-N, graphite-N (a nitrogen atom replacing a graphitic carbon atom) and oxidized-N. Moreover, the pyridinic-N can directly bond with metal atoms and the graphite-N can mediate their neighboring carbon atoms to bond with metal atoms, which can facilitate the deposition of $Co_3O_4$. The results affirmed that the composite material contains nitrogen elements introduced by carbamide, accounting for about 1.74% of the atomic weight (Table 2). Due to the higher electronegativity and smaller diameter of nitrogen than that of carbon, doping of nitrogen in graphene is beneficial for the introduced defects and more active sites toward lithium storage.[42]

### 2.2. Electrochemical performance analysis

To investigate the electrochemical performance of the $Co_3O_4$/N-HPGC nanocomposite as an anode for LIBs, the galvanostatic charge–discharge curves at a current density of 0.1 A $g^{-1}$ in the voltage range from 0.01 to 3.0 V have been measured. The first charge and discharge curves of $Co_3O_4$/N-HPGC composite electrodes with different $Co_3O_4$ loads are shown in Fig. 6a, the specific capacity and coulomb efficiency are listed in Table 3. According to results, the first charge and discharge capacity of $Co_3O_4$/N-HPGC electrodes gradually decreases with the increasing of $Co_3O_4$, while the first coulomb efficiency continuously increases, which indicates that the introduction of $Co_3O_4$ can improve the reversibility of lithium. However, the agglomeration of overmuch $Co_3O_4$ particles will lead to the decrease of lithium storage capacity. Hence, only the right amount of $Co_3O_4$ can enhance the electrochemical performance of $Co_3O_4$/N-HPGC. And the hemispherical pore structure can not only inhibit the agglomeration of nanoparticles, but also accelerate the transfer of lithium ions, which can effectively enhance its lithium storage capacity. As shown in Fig. 6b, the rate capability of $Co_3O_4$/N-HPGC electrode in the range of 0.1–

 

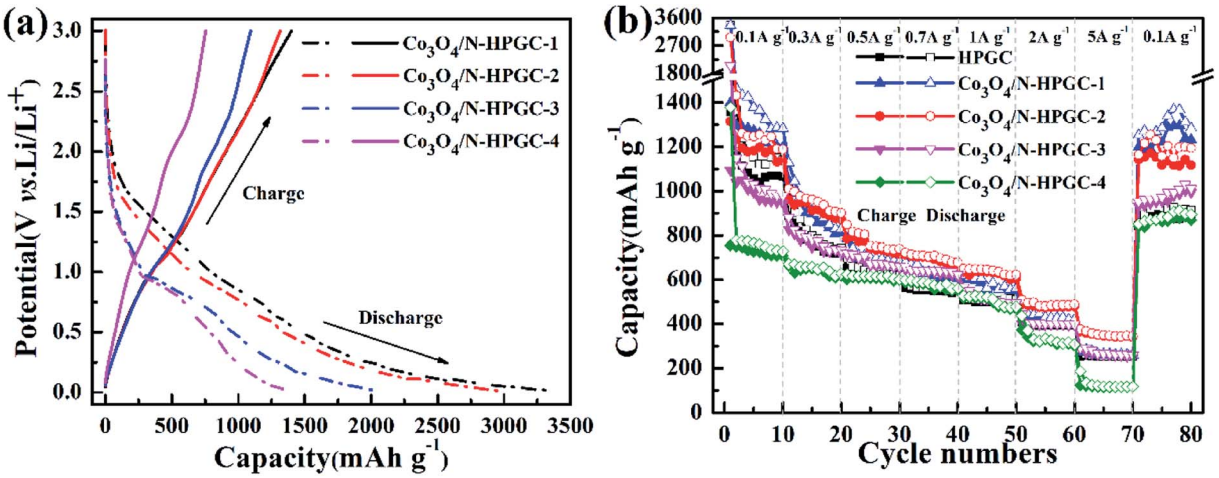


Fig. 6 (a) First charge/discharge curves at a current density of 0.1 A $g^{-1}$ and (b) rate performances at various current densities for $Co_3O_4$/N-HPGC composites with different $Co_3O_4$ loadings.

Table 3 First charge/discharge capacities and coulombic efficiency at a current density of 0.1 A $g^{-1}$ for $Co_3O_4$/HPGC-1, 2, 3 and 4

| Sample | Discharge capacity (mA h $g^{-1}$) | Charge capacity (mA h $g^{-1}$) | Coulomb efficiency (%) |
|---|---|---|---|
| $Co_3O_4$/N-HPGC-1 | 3356 | 1400 | 41.71 |
| $Co_3O_4$/N-HPGC-2 | 2696 | 1316 | 44.33 |
| $Co_3O_4$/N-HPGC-3 | 2055 | 1093 | 53.20 |
| $Co_3O_4$/N-HPGC-4 | 1378 | 754 | 54.73 |

5 A $g^{-1}$ is further tested, and the $Co_3O_4$/N-HPGC-2 has a higher capacity and an excellent rate capability. When the current density is set as 0.1, 0.3, 0.5, 0.7, 1.0 and 2.0 A $g^{-1}$, the reversible specific capacity of $Co_3O_4$/N-HPGC-2 stabilizes at 1188, 901, 740, 678, 623 and 488 mA h $g^{-1}$, respectively, which are shown in Table 4. Even at the high current density of 5 A $g^{-1}$, the electrode still remains at 344 mA h $g^{-1}$, which is significantly higher than HPGC (254 mA h $g^{-1}$), $Co_3O_4$/N-HPGC-1 (262 mA h $g^{-1}$), $Co_3O_4$/N-HPGC-3 (259 mA h $g^{-1}$) and $Co_3O_4$/N-HPGC-4 (116 mA h $g^{-1}$). Moreover, with the current density reset to 0.1 A $g^{-1}$, the specific capacity of $Co_3O_4$/N-HPGC-2 can maintain at 1194 mA h $g^{-1}$ higher than HPGC (913 mA h $g^{-1}$), quite reversibly.

The first three cyclic voltammetry (CV) curves of HPGC and $Co_3O_4$/N-HPGC composite materials are recorded in Fig. 7(a–d) at the scanning rate of 0.3 mV $s^{-1}$. In the first cathodic curve, the broad reduction peak at about 0.53 V can be attributed to the formation of solid electrolyte interphase (SEI) film,[43] but it disappears in the subsequent cycle. And compared with HPGC and $Co_3O_4$/N-HPGC-1, there are two new reduction peaks appearing near 0.83 V and 1.30 V in the other three nanocomposites, implying the production of CoO and metal cobalt during the reduction process, respectively.[44] Furthermore, two oxidation peaks are observed around 1.40 V and 2.22 V, which corresponds to the reaction of lithium ion with $Co_3O_4$ at different stages. And the reversible reaction of lithium is as follows:

$$Co_3O_4 + 8Li \underset{\text{Delithiation}}{\overset{\text{Lithiation}}{\Longleftrightarrow}} 3Co + 4Li_2O \quad (2)$$

The peaks intensity and the integral areas of the third cycle are very close to that of second cycle. These results show that the

Table 4 Reversible capacities at different current densities for HPGC and $Co_3O_4$/N-HPGC-1, 2, 3, 4

| | Reversible specific capacity (mA h $g^{-1}$) | | | | | | |
|---|---|---|---|---|---|---|---|
| Sample | 0.1 A $g^{-1}$ | 0.3 A $g^{-1}$ | 0.5 A $g^{-1}$ | 0.7 A $g^{-1}$ | 1 A $g^{-1}$ | 2 A $g^{-1}$ | 5 A $g^{-1}$ |
| HPGC | 1142 | 744 | 620 | 549 | 509 | 398 | 254 |
| $Co_3O_4$/N-HPGC-1 | 1282 | 828 | 682 | 628 | 561 | 420 | 262 |
| $Co_3O_4$/N-HPGC-2 | 1188 | 901 | 740 | 678 | 623 | 488 | 344 |
| $Co_3O_4$/N-HPGC-3 | 978 | 734 | 660 | 624 | 496 | 398 | 259 |
| $Co_3O_4$/N-HPGC-4 | 729 | 628 | 603 | 561 | 478 | 308 | 116 |

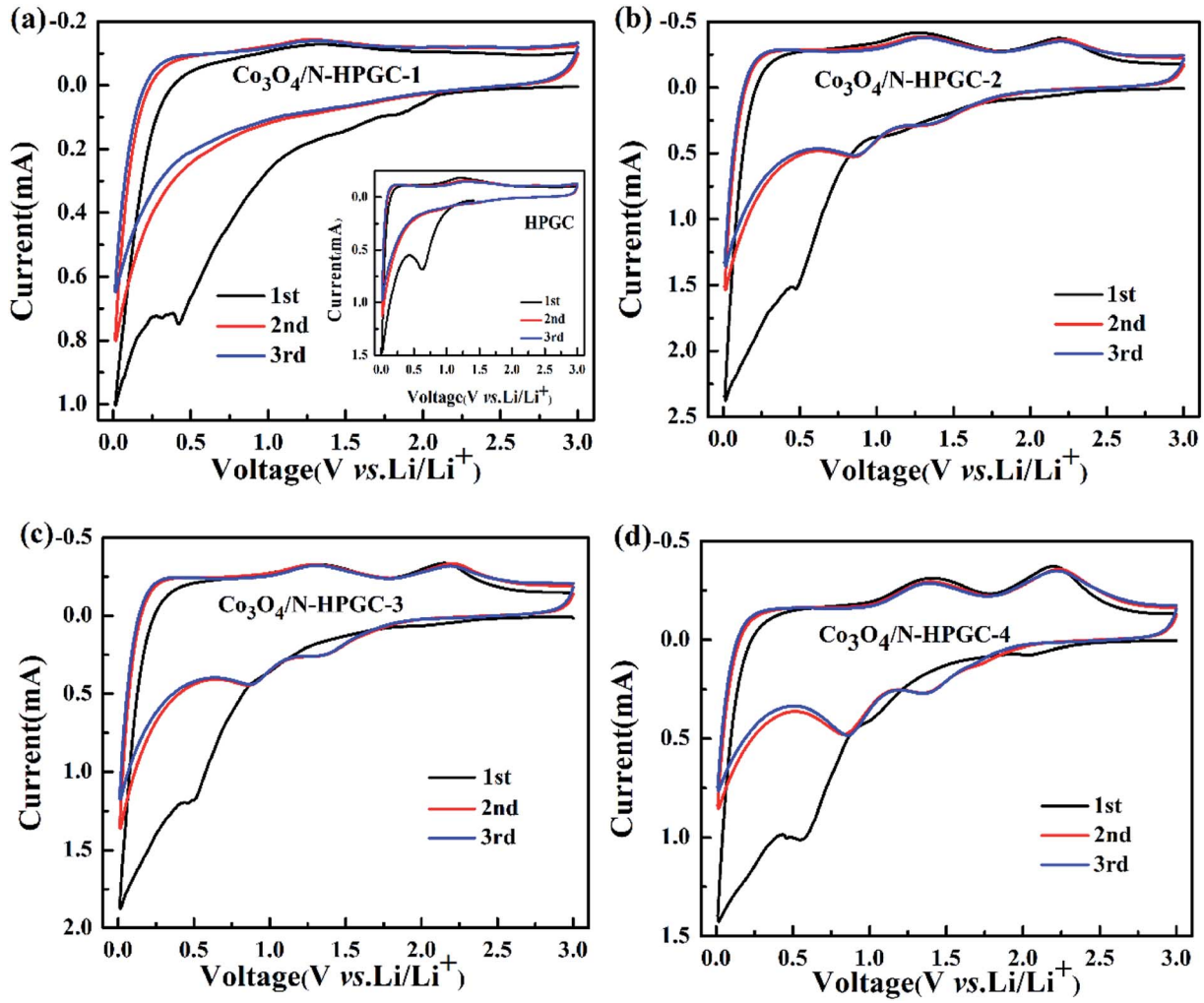


Fig. 7 Cycle voltammetry curves of HPGC, $Co_3O_4$/N-HPGC-1, 2, 3 and 4 (a–d) with different $Co_3O_4$ loadings.

electrochemically reversibility of the $Co_3O_4$/N-HPGC composite is gradually improve after the first cycle.

In order to get further comprehension about the electrochemical process, the electrochemical impedance spectroscopy (EIS) is performed, which can evaluate the electrical conductivity and lithium ions transfer of the fabricated electrodes. Fig. 8a indicates that all EIS spectra contain a broad semicircle at high frequencies demonstrating the charge transfer at the electrode/electrolyte interface, and consist of a sloped line at low frequencies, which is assigned to the lithium ions diffusion at the solid state in the electrodes.[44] Obviously, the radius of the semicircle at high frequency region for the $Co_3O_4$/N-HPGC-2 nanocomposite is much smaller than that for the other composite materials. The diminution of the semicircle demonstrates a substantial decline of charge transfer resistance due to the presence of hierarchical pore structure,[45] and the doping of N element is beneficial to the transfer of lithium ions owing to its higher electronegativity. Moreover, EIS spectra exhibit an increase of the slopes of the lines in low-frequency region, illustrating an improvement of the lithium lithiation/delithiation kinetics in the $Co_3O_4$/N-HPGC-2 anode. According to the equivalent circuit fitting values (Table 5), the $R_{SEI}$ (29.2 Ω) and $R_{ct}$ (5.3 Ω) of $Co_3O_4$/N-HPGC-2 are significantly below the HPGC (52.0 and 6.0 Ω, Fig. S3†) $Co_3O_4$/N-HPGC-1 (32.6 and 13.5 Ω), $Co_3O_4$/N-HPGC-3 (50.6 and 22.5 Ω), and $Co_3O_4$/N-HPGC-4 (51.1 and 27.4 Ω), which affirms that the $Co_3O_4$/N-HPGC-2 nanocomposite possess better electrical conductivity. The equivalent circuit used for fitting impedance spectra is shown in Fig. S2,† where $R_e$ refers to the electrolyte resistance, $R_{SEI}$ and $C_{SEI}$ are the resistance and capacitor of the surface film formed on the electrodes, $R_{ct}$ and $C_{dl}$ are the double-layer charge-

Table 5 Values of the equivalent circuit components used for fitting the experimental curve

| Sample | $R_e$ (Ω) | $R_{SEI}$ (Ω) | $R_{ct}$ (Ω) |
|---|---|---|---|
| HPGC | 2.4 | 52.0 | 6.0 |
| $Co_3O_4$/N-HPGC-1 | 1.8 | 32.6 | 13.5 |
| $Co_3O_4$/N-HPGC-2 | 2.2 | 29.2 | 5.3 |
| $Co_3O_4$/N-HPGC-3 | 1.9 | 50.6 | 22.5 |
| $Co_3O_4$/N-HPGC-4 | 2.1 | 51.1 | 27.4 |

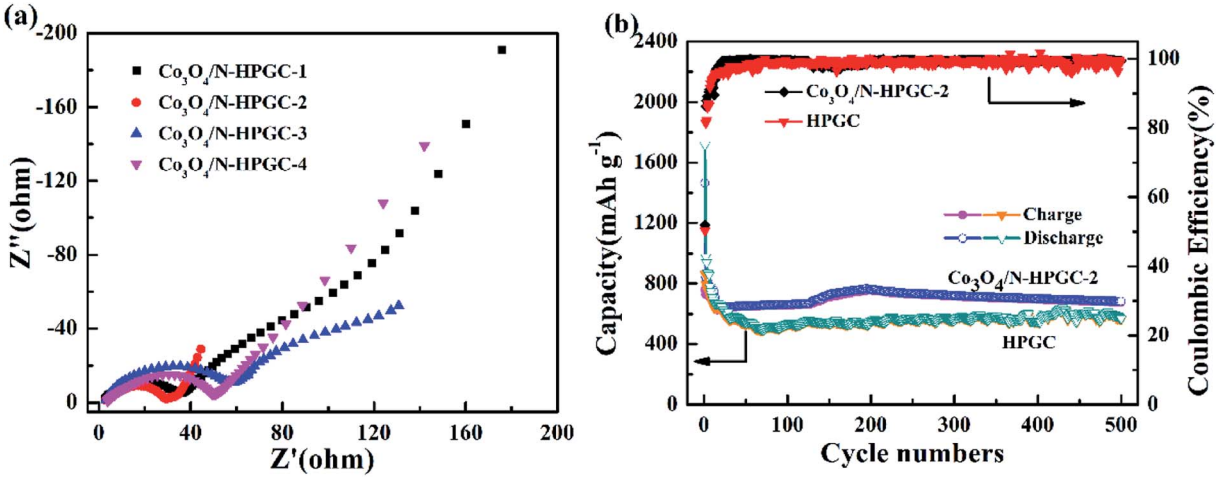


Fig. 8 (a) Nyquist plots of $Co_3O_4$/N-HPGC composites with different $Co_3O_4$ loadings (b) cycle performance at a current density of 1 A $g^{-1}$ for HPGC and $Co_3O_4$/N-HPGC-2.

transfer resistance and capacitance, and $Z_w$ is the Warburg impedance related to the diffusion of lithium ions into the bulk of the electrodes.[46]

As shown in Fig. 8b, in order to further validate the excellent electrochemical performance of $Co_3O_4$/N-HPGC-2 electrode, its cycling performance is evaluated under the current density of 1 A $g^{-1}$. It can be observed that $Co_3O_4$/N-HPGC-2 has a high initial charge–discharge capacity of 758 mA h $g^{-1}$ and 1464 mA h $g^{-1}$ respectively, and the coulomb efficiency is about 52%. At the 16th cycle, the reversible specific capacity decreases to the minimum of 644 mA h $g^{-1}$, which can be attributed to the formation of SEI membrane and the irreversible transformation of $Co_3O_4$. The reversible specific capacity increases to the maximum of 768 mA h $g^{-1}$ at the 195th cycle due to the continuous activation of the composite electrode. Additionally, at the 500th cycle, its reversible specific capacity stabilizes at 683 mA h $g^{-1}$, much higher than that of HPGC electrode (568 mA h $g^{-1}$) after 500 cycles at the current density of 1 A $g^{-1}$. Moreover, the coulombic efficiency of $Co_3O_4$/N-HPGC-2 electrode rise to more than 98% from the 18th cycle, suggesting the right amount of $Co_3O_4$ loads can significantly enhance its electrochemical properties, which is mainly ascribed to the synergistical effects of the $Co_3O_4$ nanoparticles, the hemispherical porous structure and the N-containing functional groups on the $Co_3O_4$/N-HPGC nanocomposites.[47] The 3D hemispherical superimposed structure of graphene with uniformly loaded $Co_3O_4$ nanoparticles not only can prevent further stack of graphene, but also can restrain the combination of $Co_3O_4$ particle, inhibit the circulation volume change and accelerate electron transfer during the charge–discharge process, thereby enhancing the lithium storage capacity and cycle stability of the composite electrode.[48]

Recently, many electrode nanomaterials have been explored based on carbon-based materials and $Co_3O_4$, and all of them have some advantages and limitations. A comparison of the performance of our newly designed $Co_3O_4$/N-HPGC with those already reported in literature is shown in Table 6. Through comparison, it can be clearly seen that the as-prepared nanocomposites result in a relatively high reversible capacity (683 mA h $g^{-1}$ after 500 cycles) based on the large current density at 0.1 A $g^{-1}$.

In addition, the nitrogen-containing functional groups of the nanocomposites also play a significant role in enhancing the electrochemical properties of the $Co_3O_4$/N-HPGC electrodes. And the doped nitrogen element can introduce the donor states near the Fermi level to generate n-type conductive materials, the N element configuration provides much more available active sites and nucleation sites to strengthen the binding energy between the metal oxides and carbon-based materials, which is beneficial to promoting the adhesion of electrolyte ions onto the electrode surface and decreasing the charge transfer resistance.[50] Therefore, a conductive network is generated because of the homogeneous dispersion of the $Co_3O_4$ particles on the surface and internal hemispheric pore sites of the $Co_3O_4$/N-HPGC nanomaterials, which can effectively enhance its capacitance. Furthermore, the nitrogen-containing functional

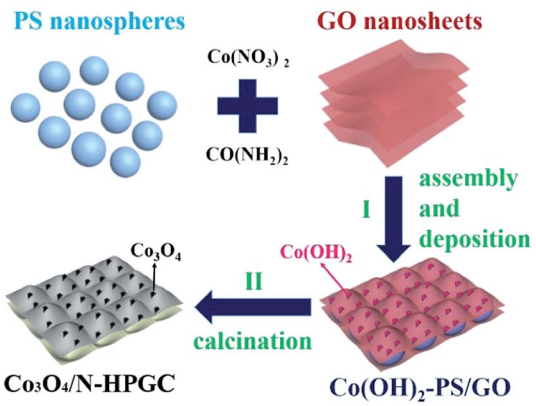


Fig. 9 Schematic illustration of the preparation approach to $Co_3O_4$/N-HPGC.

Table 6 Comparison of the performance of $Co_3O_4$/N-doped carbon-based nanocomposites as anode materials for lithium ion batteries

| Active materials | Current density A $g^{-1}$ | Reversible capacity mA h $g^{-1}$ | Cycle numbers | Initial coulombic efficiency (%) | Ref. |
|---|---|---|---|---|---|
| $Co_3O_4$/N-HPGC-2 | 0.1 | 683 | 500 | 52.0 | This work |
| $Co_3O_4$@N–C nanotubes | 0.1 | 598 | 50 | 72 | 41 |
| Porous $Co_3O_4$/N–C | 1 | 579.3 | 200 | 51 | 49 |
| N–C/$Co_3O_4$ | 0.1 | 983.9 | 100 | 54.7 | 35 |
| $Co_3O_4$/N-doped GN | 0.2 | 950 | 100 | No | 45 |

groups on the nanocomposite react with lithium by forming $Li_3N$:

$$3Li + N \rightarrow Li_3N, \quad (3)$$

and the reaction is quasi-reversible:[51,52]

$$4Co + Li_3N \rightleftharpoons Co + Co_3N + 3Li. \quad (4)$$

Meanwhile, the anchored $Co_3O_4$ on the composites can generate metallic cobalt owing to the electrochemical reduction reaction, which can further catalyze the decomposition of $Li_3N$ and produce lithiated cobalt nitride possessing high lithium storage capacity. Thus, the nitrogen-containing functional groups and $Co_3O_4$ nanoparticles on the $Co_3O_4$/N-HPGC can synergistically facilitate the lithium-ions storage capacity.[35]

# 3. Experimental

## 3.1. Chemicals and reagents

Flake graphite of chemical grade (≤30 μm) were from Sinopharm Chemical Reagent Co. Ltd., China. Styrene, ethanol and sodium p-styrene sulfonate were obtained from Kelong chemical reagent company. Cobalt nitrate hexahydrate was bought from Shanghai Macklin Biochemical Co. Ltd. All other reagents used in this study, including ethylenediamine, sodium bicarbonate, potassium persulfate, sodium chloride, sodium hydroxide, sodium nitrate, concentrated sulfuric acid, potassium permanganate, concentrate hydrochloric acid, hydrogen peroxide, absolute ethyl ethanol and carbamide were purchased from Luoyang Chemical Reagent Co. Ltd., China. All these chemicals were of analytical grade and were used without further purification. Water used in the experiments was double-distilled.

## 3.2. Preparation of PS colloidal microspheres

The first step was the pretreatment of styrene monomer in order to obtain the purified styrene. In a typical procedure, sodium hydroxide (5 wt%) was added into the styrene solution in a separatory funnel to remove the polymerization inhibitor recognized as a phenolic compound through shaking the mixed solution, which was defined as extraction separation. The above operation was repeated three times. The solution treated by extraction separation was then placed into a distilling flask for further purification through decompressing distillation, and eventually the purified styrene was obtained. The PS colloidal microspheres were fabricated through emulsion polymerization as described below. The deionized water was first added into the jacketed reactor connected with the thermostatic water bath for controlling the reaction temperature. Styrene as the monomer, sodium bicarbonate as the stabilizer, and sodium p-styrene sulfonate as the emulsifier were then added into the reactor maintaining stirring at 80 °C for 1 h. Subsequently, the potassium persulfate served as the initiator was added to the emulsion and kept the reaction for another 18 h. Finally, monodispersed PS colloidal microspheres were prepared, which appeared bright milky white.

## 3.3. Preparation of $Co_3O_4$/N-HPGC nanocomposites

Graphene oxide (GO) was prepared through the modified Hummers method. Then, the prepared GO suspension (3 mg $mL^{-1}$) and PS microspheres emulsion (60 mg $mL^{-1}$, about 112 nm) were mixed and ultrasonically dispersed for 30 min. Took 120 mL of the above mixed suspension into 250 mL beaker, then slowly added cobalt nitrate solution (1 mol $L^{-1}$), 0.36 g of carbamide and 6 mL PS microsphere emulsion were slowly added into the mixture suspension successively, continuously stirring for 15 min and ultrasonicated for 15 min. Subsequently, the mixed solution was transferred to a Teflon lined stainless steel reaction vessel, heated up to 120 °C at the heating rate of 2 °C $min^{-1}$, and then maintained at this temperature for 12 h before naturally cooled to room temperature. Afterwards the content was washed with ethanol solution for three times and the product was freeze-dried at −60 °C. Finally, the prepared precursor was calcined at 500 °C for 2 h in a tube furnace under nitrogen protection at the heating rate of 5 °C $min^{-1}$ to obtain the $Co_3O_4$/N-HPGC composite. The above operation was repeated to obtain the nanocomposites with different volumes of cobalt nitrate solution (0, 0.375, 0.75, 1.5 and 3.0 mL), which were denoted as HPGC, $Co_3O_4$/N-HPGC-1, 2, 3, 4, respectively. Furthermore, the fabrication process for $Co_3O_4$/N-HPGC is illustrated in Fig. 9.

## 3.4. Characterization

The structure and morphology of $Co_3O_4$/N-HPGC were investigated using a JEM-2100 transmission electron microscope (TEM, JEOL, Japan). The elemental analysis of samples was determined by X-ray photoelectron spectra (XPS) on a VG Escalab 250 spectrometer (Thermo Scientific, USA). The X-ray diffraction (XRD) patterns were obtained by a D8 Advance X-ray diffractometer (Bruker, Germany) equipped with a Cu Kα

 

radiation source ($\lambda$ = 0.15418 nm) at a scanning rate of 5° $min^{-1}$. $N_2$ adsorption–desorption isotherms were measured using a Quantachrome Autosorb-iQ-MP (USA) analyzer at −196 °C with a relative pressure ranging from 0.0112 to 0.9948. The specific surface area was calculated by the Brunauer–Emmett–Teller (BET) model.

### 3.5. Electrochemical measurements

The electrochemical performances of the $Co_3O_4$/N-HPGC nanocomposites were evaluated by assembling them into CR2016 button-type cells. The working electrodes were prepared as follows: a slurry was synthesized by blending $Co_3O_4$/N-HPGC active materials (0.08 g, 80 wt%), conductive acetylene black (0.01 g, 10 wt%) and polyvinylidene fluoride (PVDF) adhesive (0.01 g, 10 wt%) in *N*-methyl-2-pyrrolidone (NMP) solvent. Then the prepared slurry was coated on the surface of copper foils, the foliated coppers were dried at 120 °C under vacuum for 10 h to remove the excess solvent, and the obtained electrodes were cut into disks with the diameter of 14 nm. The cells were assembled in an argon-filled glovebox (with less than 1 ppm of oxygen and water vapor), using lithium foils as the counter electrode and reference electrode, Celgard 2400 microporous polypropylene membrane as the separator, and a solution of 1 M $LiPF_6$ in a mixture of ethylene carbonate (EC)–dimethyl carbonate (DMC) (1 : 1 by volume) as the electrolyte. The galvanostatic charge–discharge (GCD) experiments were tested by Neware BTS 4000 batteries testing system at cycling rates ranging from 0.1 A $g^{-1}$ to 5 A $g^{-1}$, between 0.01 and 3.0 V at ambient temperature. Cyclic voltammetry (CV) measurement was performed at a scan rate of 0.3 mV $s^{-1}$ with a voltage of 0.01–3.0 V (*vs.* $Li^+$/Li) using an electrochemical working station (RST5200F, Shiruisi Co. Zhengzhou). And the electrochemical impedance spectroscopy (ESI) experiment of the as-pared composites was carried out using a Princeton PARSTAT 2273 (USA) electrochemical workstation in the frequency range of 50 to $10^5$ Hz.

## 4. Conclusions

In summary, the $Co_3O_4$/N-HPGC nanocomposites were synthesized by a hydrothermal-template approach with polystyrene (PS) microspheres as the template. As shown in the aforementioned results, the $Co_3O_4$ nanoparticles are uniformly loaded on the graphene sheets of $Co_3O_4$/N-HPGC composite material, and the prepared $Co_3O_4$/N-HPGC nanohybrid has a large specific area (348 $m^2$ $g^{-1}$), rich hemisphere-porous structure, successful nitrogen doping and high electrical conductivity. It has been observed that the $Co_3O_4$/N-HPGC nanocomplex is a prospective anode material for LIBs due to its enhancive reversible specific capacity, outstanding cyclic performance and excellent rate capability. Meanwhile, the improved electrochemical performance is ascribed to the synergistic effects of the nanoscale $Co_3O_4$ particles, the hemispherical porous structure and the nitrogen-containing functional groups of the nanocomposites. Under the current density of 0.1 A $g^{-1}$, the reversible specific capacity of $Co_3O_4$/N-HPGC-2 with suitable loads of $Co_3O_4$ is as high as 1188 mA h $g^{-1}$. And its capacity remains at 344 mA h $g^{-1}$ under 5 A $g^{-1}$, even can maintain 683 mA h $g^{-1}$ after 500 cycles the current density of 1 A $g^{-1}$, which offers a possibility to synthesize nanostructure electrode materials for energy storage.

## Conflicts of interest

There are no conflicts to declare.

## Acknowledgements

This work was supported by the National Natural Science Foundation of China (U1803114), the Education Department Science Foundation of Henan Province (19A530002, 19A440002), the National Key Research Plan (2018YFB0604500) and the China Postdoctoral Science Foundation (207500).

## References

1 J. G. Wang, F. Kang and B. Wei, Engineering of $MnO_2$-based nanocomposites for high-performance supercapacitors, *Prog. Mater. Sci.*, 2015, **74**, 51–124.
2 Y. Li, B. Xu, H. Xu, H. Duan, X. Lü, S. Xin, W. Zhou, L. Xue, G. Fu and A. Manthiram, Hybrid Polymer/Garnet Electrolyte with a Small Interfacial Resistance for Lithium-Ion Batteries, *Angew. Chem.*, 2017, **56**(3), 753–756.
3 Y. Zhang, Y. Pan, Y. Chen, B. L. Lucht and A. Bose, Towards reducing carbon content in silicon/carbon anodes for lithium ion batteries, *Carbon*, 2017, **112**, 72–78.
4 I. Capone, K. Hurlbutt, A. J. Naylor, A. W. Xiao and M. Pasta, Effect of the Particle-Size Distribution on the Electrochemical Performance of a Red Phosphorus-Carbon Composite Anode for Sodium-Ion Batteries, *Energy Fuels*, 2019, **33**(5), 4651–4658.
5 L. Z. Bai, D.-L. Zhao, T.-M. Zhang, W.-G. Xie, J.-M. Zhang and Z.-M. Shen, A comparative study of electrochemical performance of graphene sheets, expanded graphite and natural graphite as anode materials for lithium-ion batteries, *Electrochim. Acta*, 2013, **107**(2), 555–561.
6 Y. Lu, Q. Zhang, L. Li, Z. Niu and J. Chen, Design Strategies toward Enhancing the Performance of Organic Electrode Materials in Metal-Ion Batteries, *Chem*, 2018, **4**, 2786–2813.
7 C. Luo, O. Borodin, X. Ji, S. Hou, K. J. Gaskell, X. Fan and C. Wang, Azo compounds as a family of organic electrode materials for alkali-ion batteries, *Proc. Natl. Acad. Sci. U. S. A.*, 2018, **115**(9), 2004–2009.
8 M. Zheng, H. Tang, L. Li, Q. Hu, L. Zhang, H. Xue and H. Pang, Hierarchically Nanostructured Transition Metal Oxides for Lithium-Ion Batteries, *Adv. Sci.*, 2018, **5**(3), 1700592.
9 F. Zhang and L. Qi, Recent Progress in Self-Supported Metal Oxide Nanoarray Electrodes for Advanced Lithium-Ion Batteries, *Adv. Sci.*, 2016, **3**(9), 1600049.
10 W. Li, L. Zeng, Y. Wu and Y. Yu, Nanostructured electrode materials for lithium-ion and sodium-ion batteries via electrospinning, *Sci. China Mater.*, 2016, **59**(4), 287–321.

11 Y. Jiang, Y. Xue, X. Wei, T. Ming and G. Lin, $Co_3O_4$-graphene nanoflowers as anode for advanced lithium ion batteries with enhanced rate capability, *J. Alloys Compd.*, 2017, **710**, 114–120.

12 Q. Qu, G. Tian, H. Zheng, X. Li, H. Liu, S. Ming, S. Jie and H. Zheng, Graphene oxides-guided growth of ultrafine $Co_3O_4$ nanocrystallites from MOFs as high-performance anode of Li-ion batteries, *Carbon*, 2015, **92**, 119–125.

13 M. Liu, D. Xia, Y. Ma, W. Xie, X. Hou, Y. Fu and D. He, Well-designed hierarchical $Co_3O_4$ architecture as a long-life and ultrahigh rate capacity anode for advanced lithium-ion batteries, *Adv. Mater. Interfaces*, 2017, **4**(19), 1700553.

14 M. V. Reddy, G. V. Subba Rao and B. V. Chowdari, Metal oxides and oxysalts as anode materials for Li ion batteries, *Chem. Rev.*, 2013, **113**(7), 5364–5457.

15 G. Jin, C. Lei, Z. Xiao and C. Hao, Porous $Co_3O_4$ nanorods as anode for lithium-ion battery with excellent electrochemical performance, *J. Solid State Chem.*, 2014, **213**, 193–197.

16 J. Xu, J. Wu, L. Luo, X. Chen, H. Qin, V. Dravid, S. Mi and C. Jia, $Co_3O_4$ nanocubes homogeneously assembled on few-layer graphene for high energy density lithium-ion batteries, *J. Power Sources*, 2015, **274**, 816–822.

17 Y. Lou, L. Jing, Y. Peng and J. Chen, Ultra-small $Co_3O_4$ nanoparticles-reduced graphene oxide nanocomposite as superior anodes for lithium-ion batteries, *Phys. Chem. Chem. Phys.*, 2015, **17**(14), 8885–8893.

18 G. Huang, F. Zhang, X. Du, Y. Qin, D. Yin and L. Wang, Metal organic frameworks route to in situ insertion of multiwalled carbon nanotubes in $Co_3O_4$ polyhedra as anode materials for lithium-ion batteries, *ACS Nano*, 2015, **9**(2), 1592–1599.

19 P. Zhu, Z. Yang, P. Zeng, J. Zhong, J. Yu and J. Cai, Homogeneous precipitation synthesis and electrochemical performance of $LiFePO_4$/CNTs/C composites as advanced cathode materials for lithium ion batteries, *RSC Adv.*, 2015, **5**(130), 107293–107298.

20 F. Ning, M. Shao, C. Zhang, S. Xu, M. Wei and X. Duan, $Co_3O_4$@layered double hydroxide core/shell hierarchical nanowire arrays for enhanced supercapacitance performance, *Nano Energy*, 2014, **7**, 134–142.

21 Z. Zhang, L. Gao, Y. Dong, J. Zhao and Z. Wu, Embedding $Co_3O_4$ nanoparticles into graphene nanoscrolls as anode for lithium ion batteries with superior capacity and outstanding cycling stability, *Prog. Nat. Sci.: Mater. Int.*, 2018, **28**(2), 212–217.

22 R. Raccichini, A. Varzi, S. Passerini and B. Scrosati, The role of graphene for electrochemical energy storage, *Nat. Mater.*, 2015, **14**(3), 271–279.

23 N. Venugopal, J. Yoo and W.-S. Yoon, A Simple Synthesis of $Co_3O_4$ Nanoparticles Decorated on Multiwalled Carbon Nanotubes Hybrid Material for Rechargeable Li-Ion and Li-Air Batteries, *J. Nanosci. Nanotechnol.*, 2017, **17**(5), 3390–3396.

24 Y. Dou, J. Xu, B. Ruan, Q. Liu, Y. Pan, Z. Sun and S. X. Dou, Atomic Layer-by-Layer $Co_3O_4$/Graphene Composite for High Performance Lithium-Ion Batteries, *Adv. Energy Mater.*, 2016, **6**(8), 1501835.

25 H. Suna, Y. Liuc, Y. Yud, M. Ahmade, N. Ding and Z. Jing, Mesoporous $Co_3O_4$ nanosheets-3D graphene networks hybrid materials for high-performance lithium ion batteries, *Electrochim. Acta*, 2014, **118**, 1–9.

26 Z. Wang, X. Xiong, L. Qie and Y. Huang, High-performance lithium storage in nitrogen-enriched carbon nanofiber webs derived from polypyrrole, *Electrochim. Acta*, 2013, **106**, 320–326.

27 L. Qie, W. M. Chen, Z. H. Wang, Q. G. Shao, X. Li, L. X. Yuan, X. L. Hu, W. X. Zhang and Y. H. Huang, Nitrogen-doped porous carbon nanofiber webs as anodes for lithium ion batteries with a superhigh capacity and rate capability, *Adv. Mater.*, 2012, **24**(15), 2047–2050.

28 Y. Mao, H. Duan, B. Xu, L. Zhang, Y. Hu, C. Zhao, Z. Wang, L. Chen and Y. Yang, Lithium storage in nitrogen-rich mesoporous carbon materials, *Energy Environ. Sci.*, 2012, **5**(7), 7950.

29 M. Liu, X. Hou, T. Wang, Y. Ma, K. Sun, D. Liu, Y. Wang, D. He and J. Li, Rapid activation and enhanced cycling stability of $Co_3O_4$ microspheres decorated by N-doped amorphous carbon shell for advanced LIBs, *Electrochim. Acta*, 2018, **283**, 979–986.

30 J. Fan, Y. Fan, R. Wang, S. Xiang, H. Tang and S. Sun, A Novel Strategy for Sulfur−Doped Carbon Nanotube as a High-Efficient Pt Catalyst Support toward Methanol Oxidation Reaction, *J. Mater. Chem. A*, 2017, **5**, 19467–19475.

31 G. X. Pan, X. H. Xia, F. Cao, J. Chen and Y. J. Zhang, Construction of Co/$Co_3O_4$-C ternary core-branch arrays as enhanced anode materials for lithium ion batteries, *J. Power Sources*, 2015, **293**, 585–591.

32 J. Xiang, W. Lv, C. Mu, J. Zhao and B. Wang, Activated Hard Carbon from Orange Peel for Lithium/Sodium Ion Battery Anode with Long Cycle Life, *J. Alloys Compd.*, 2017, **701**, 870–874.

33 C. Tang, Q. Zhang, M. Zhao, J. Huang, X. Cheng, G. Tian, H. Peng and F. Wei, Nitrogen-Doped Aligned Carbon Nanotube/Graphene Sandwiches: Facile Catalytic Growth on Bifunctional Natural Catalysts and Their Applications as Scaffolds for High-Rate Lithium-Sulfur Batteries, *Adv. Mater.*, 2014, **26**, 6100–6105.

34 L. Zhuo, Y. Wu, J. Ming, L. Wang, Y. Yu, X. Zhang and F. Zhao, Facile Synthesis of a $Co_3O_4$-Carbon Nanotube Composite and its Superior Performance as an Anode Material for Li-Ion Batteries, *J. Mater. Chem. A*, 2013, **1**, 1141–1147.

35 L. Guo, Y. Ding, C. Qin, W. Li, J. Du, Z. Fu, W. Song and F. Wang, Nitrogen-doped porous carbon spheres anchored with $Co_3O_4$ nanoparticles as high-performance anode materials for lithium-ion batteries, *Electrochim. Acta*, 2016, **187**, 234–242.

36 Y. Liu, Z. Cheng, H. Sun, H. Arandiyan, J. Li and M. Ahmad, Mesoporous $Co_3O_4$ sheets/3D graphene networks nanohybrids for high-performance sodium-ion battery anode, *J. Power Sources*, 2015, **273**, 878–884.

37 A. Li, Z. Ming, S. Wei, C.-P. Wang and X.-H. Bu, Facile Synthesis of $Co_3O_4$ Nanosheets from MOFs Nanoplates for

 

High Performance Anode of Lithium-Ion Batteries, *Inorg. Chem. Front.*, 2018, **5**, 1602–1608.

38 N. Yang, J. Liu, Y. Sun and Y. Zhu, Au@PdOx with a PdOx-rich shell and Au-rich core embedded in $Co_3O_4$ nanorods for catalytic combustion of methane, *Nanoscale*, 2017, **9**(6), 2123–2128.

39 J. M. Xu, J. S. Wu, L. L. Luo, X. Q. Chen, H. B. Qin, V. Dravid, S. B. Mi and C. L. Jia, $Co_3O_4$ nanocubes homogeneously assembled on few-layer graphene for high energy density lithium-ion batteries, *J. Power Sources*, 2015, **274**, 816–822.

40 L. Wang, Y. L. Zhang, X. H. Wang, S. H. Chen, F. G. Xu, L. Zuo, J. F. Wu, L. L. Sun, Z. Li, H. Q. Hou and Y. H. Song, Nitrogen-Doped Porous Carbon/$Co_3O_4$ Nanocomposites as Anode Materials for Lithium-Ion Batteries, *ACS Appl. Mater. Interfaces*, 2014, **6**, 7117–7125.

41 K. Xie, P. Wu, Y. Zhou, Y. Ye, H. Wang, Y. Tang, Y. Zhou and T. Lu, Nitrogen-doped carbon-wrapped porous single-crystalline CoO nanocubes for high-performance lithium storage, *ACS Appl. Mater. Interfaces*, 2014, **6**(13), 10602–10607.

42 H. Sun, S. Xiang, H. Tao, M. Yu, F. Lu and L. Jie, Graphene-Wrapped Mesoporous Cobalt Oxide Hollow Spheres Anode for High-Rate and Long-Life Lithium Ion Batteries, *J. Phys. Chem. C*, 2014, **118**(5), 2263–2272.

43 Q. Su, W. Yuan, L. Yao, Y. Wu, J. Zhang and G. Du, Microwave-assisted synthesis of $Co_3O_4$-graphene sheet-on-sheet nanocomposites and electrochemical performances for lithium ion batteries, *Mater. Res. Bull.*, 2015, **72**, 43–49.

44 F. Xiang, R. Mukherjee, J. Zhong, Y. Xia, N. Gu, Z. Yang and N. Koratkar, Scalable and rapid Far Infrared reduction of graphene oxide for high performance lithium ion batteries, *Energy Storage Materials*, 2015, **1**, 9–16.

45 L. Lai, J. Zhu, Z. Li, D. Y. W. Yu, S. Jiang, X. Cai, Q. Yan, Y. M. Lam, Z. Shen and J. Lin, $Co_3O_4$/nitrogen modified graphene electrode as Li-ion battery anode with high reversible capacity and improved initial cycle performance, *Nano Energy*, 2014, **3**, 134–143.

46 X. Zhu, G. Ning, X. Ma, Z. Fan, C. Xu, J. Gao, C. Xu and F. Wei, High Density $Co_3O_4$ Nanoparticles Confined in a Porous Graphene Nanomesh Network Driven by an Electrochemical Process: Ultra-high Capacity and Rate Performance for Lithium Ion Batteries, *J. Mater. Chem. A*, 2013, **1**, 14023–14030.

47 S. Yang, X. Song, P. Zhang and L. Gao, Facile synthesis of nitrogen-doped graphene-ultrathin $MnO_2$ sheet composites and their electrochemical performances, *ACS Appl. Mater. Interfaces*, 2013, **5**(8), 3317–3322.

48 S. S. Li, H. P. Cong, P. Wang and S. H. Yu, Flexible nitrogen-doped graphene/carbon nanotube/$Co_3O_4$ paper and its oxygen reduction activity, *Nanoscale*, 2014, **6**(13), 7534–7541.

49 X. Han, W.-M. Chen, X. Han, Y.-Z. Tan and D. Sun, Nitrogen-rich MOF derived porous $Co_3O_4$/NeC composites with superior performance in lithium-ion batteries, *J. Mater. Chem.*, 2016, **4**, 13040–13045.

50 L. Wang, Y. Zheng, X. Wang, S. Chen, F. Xu, L. Zuo, J. Wu, L. Sun, Z. Li, H. Hou and Y. Song, Nitrogen-doped porous carbon/$Co_3O_4$ nanocomposites as anode materials for lithium-ion batteries, *ACS Appl. Mater. Interfaces*, 2014, **6**(10), 7117–7125.

51 W. Bao, B. Yu, W. Li, H. Fan, J. Bai and Z. Ren, $Co_3O_4$/nitrogen-doped graphene/carbon nanotubes: An innovative ternary composite with enhanced electrochemical performance, *J. Alloys Compd.*, 2015, **647**, 873–879.

52 Y. P. Wu, Effects of nitrogen on the carbon anode of a lithium secondary battery, *Solid State Ionics*, 1999, **120**(120), 117–123.